analytical chemistry

pubs.acs.org/ac Article

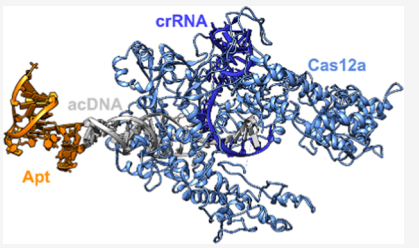
Aptamer-Linked CRISPR/Cas12a-Based Immunoassay

Hui Li,[‖] Menglu Li,[‖] Yucai Yang, Fei Wang, Feng Wang,* and Chao Li*

Cite This: https://dx.doi.org/10.1021/acs.analchem.0c04687 Read Online

ACCESS | Metrics & More | Article Recommendations | Supporting Information

ABSTRACT: The clustered regularly interspaced short palindromic repeat (CRISPR)/Cas system has shown great promising applications in the area of nucleic acid biosensing. However, because of the dearth of versatile signal transduction strategies, this system is usually compromised to low versatility, moderate sensitivity, and complex operation for non-nucleic acid targets, limiting its clinical transition. Herein, we describe a direct method to establish the correlation between non-nucleic acid analytes and the CRISPR/Cas12a system using a series of rationally designed, aptamer-flanked activator DNA strands, which enable ultrasensitive detection of biomarkers from different species, greatly broadening the possibility of the CRISPR/Cas system in bioanalysis. Meanwhile, the signal output is highly optional and the sensing principle is akin to the traditional enzyme-linked immunosorbent assay (ELISA), so it can be directly imposed on the currently available ELISA platform, further facilitating its application in medical diagnostics.



Downloaded via SHANGHAI NORMAL UNIV on February 2, 2021 at 11:44:17 (UTC).
See https://pubs.acs.org/sharingguidelines for options on how to legitimately share published articles.

INTRODUCTION

The clustered regularly interspaced short palindromic repeat (CRISPR) system has been widely used in the area of gene editing.[1,2] Recently, CRISPR-associated proteins have been explored to develop sensing strategies such as specific high-sensitivity enzymatic reporter unlocking (SHERLOCK)[3,4] and DNA endonuclease-targeted CRISPR trans reporter (DETECTR) because of their unique properties. For example, Cas12a from *Lachnospiraceae* bacterium ND2006 is an RNA-guided enzyme, which binds to a single-stranded guide RNA (crRNA) to recognize its target double-stranded DNA (dsDNA).[5] CRISPR-Cas12a (Cfp1) has been demonstrated to not only cleave the target dsDNA (termed cis-acting cleavage) but also indiscriminately cleave any nontarget single-stranded DNA (termed trans-acting cleavage).[6,7] Impressively, the collateral cleavage of ssDNA strands in solution by Cas12a is highly efficient (~1250 turnovers per second), so Cas12a-based detection methods usually have excellent sensitivity for the detection of nucleic acids.[8−10] Very recently, to broaden its application, some strategies have used CRISPR/Cas12a to detect other biomolecules such as small organic molecules and protein molecules.[11−14] However, these established methods usually adopt complex and inefficient signal transduction strategies since it is technically difficult to build a direct relationship between CRISPR/Cas12a systems with other non-nucleic acid targets since Cas12a has no ability to recognize these analytes directly. As a result, different recognition elements have been introduced into the Cas12a-based detection platform, and signal transduction relies on competitive binding or indirect interaction between recognition molecules and Cas12a enzymes. For example, Liang and co-workers have introduced bacterial allosteric transcription factors (aTFs) into the Cas12a-based detection platform to report small organic molecules such as uric acid and *p*-hydroxybenzoic acid. However, since Cas12a cannot bind with small molecules directly, they need to use cellulose-binding domain-fused aTFs to recognize small molecules and then release target dsDNA to activate Cas12a, which not only requires complex prokaryotic expression systems to obtain specific aTFs but also tedious protein modification and purification steps to prepare aTF/DNA-modified cellulose beads.[11] Consequently, most CRISPR/Cas12a-based detection systems suffer from moderate versatility and sensitivity, greatly limiting their real applications in biomedical diagnostics.[15]

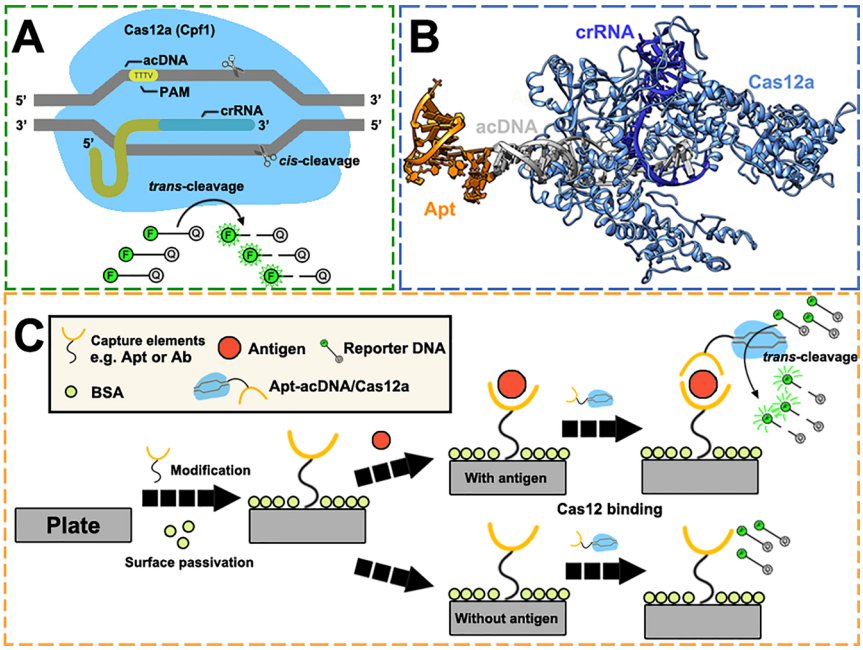
Enzyme-linked immunosorbent assay (ELISA) plays a critical role in bioassay, which is the most widely used method for antigen detection.[16] In a typical assay, analytes induce the formation of sandwich structures using a pair of antibodies. Then, the enzyme (in many cases, horseradish peroxidase (HRP)) labeled on the detection antibody can catalyze the conversion of a substrate into a colored product for signal readout. Because numerous antibodies or other newly developed specific ligands are commercially available, ELISA can be used to detect a range of analytes including protein, small antigens, and even whole cells. However, despite its widespread use, one main hurdle of traditional ELISA is its relatively poor sensitivity, usually in nanomolar/picomolar range,[17,18] because of the limited catalytic efficiency of HRP. Moreover, the preparation of HRP-linked antibodies usually needs complex chemical modification and tedious purification steps, which may hamper the function of HRP or antibodies.

Received: November 5, 2020
Accepted: January 14, 2021

ACS Publications © XXXX American Chemical Society

https://dx.doi.org/10.1021/acs.analchem.0c04687
Anal. Chem. XXXX, XXX, XXX−XXX

Scheme 1. (A) Schematic Illustration of Trans/Cis-Activity of CRISPR/Cas12a (acDNA, Activator DNA Strand; PAM, Protospacer-Adjacent Motif; crRNA, CRISPR RNA Strand); (B) Overall Three-Dimensional (3D) Structure of the Apt-acDNA/crRNA/Cas12a Complex (the Used Models of Cas12a (ID: 6I1K) and Apt (ID: 1RDE) Were Obtained from the Protein Data Bank (PDB) and Imaged by Chimera Software, Version 1.11); and (C) Whole Workflow of the Proposed ALCIA for Antigen Detection



Hence, traditional ELISA has been far from enough to satisfy the increasing demands for disease diagnostic since many antigens found in clinical samples are in the sub-picomolar or femtomolar range at the early stage of the disease.

Inspired by the above arguments, we wonder whether the CRISPR/Cas12a system can be directly introduced into ELSIA, which may combine the advantages of the two techniques. In this work, we demonstrate this idea and design an aptamer-linked CRISPR/Cas12-based immunoassay (denoted ALCIA) for highly sensitive detection of a variety of analytes using desired signal readout, which greatly expands the application of the CRISPR-Cas12 system in medical diagnostics. To do so, we rationally repurpose the activator DNA (acDNA) of Cas12a, in which is simply added with an analyte-targeting aptamer sequence at the 5′ end (termed as Apt-acDNA, Table S1). The aptamer is known as a chemical antibody that can recognize a wide range of analytes with many advantages such as high affinity, low cost, easy synthesis, and good stability.[19] Consequently, when Apt-acDNA binds to the crRNA/Cas12a complex through nucleic acid hybridization, the resulting complex possesses two important functions at the same time, namely, molecule recognition and signal generation, which do not involve any complex chemical modification or purification. Furthermore, through analysis of the potential structure of the ternary complex (Scheme 1B), the activity site of trans-cleavage is not affected, which is very beneficial to its subsequent use in bioanalysis.

The whole workflow of the proposed ALCIA is shown in Scheme 1C. By utilizing this technique, ALCIA has several attractive features: (1) it is highly versatile and greatly broadens the application of the CRISPR/Cas12a system in bioanalysis, which can be used to detect various analytes without complex design and chemical modification; (2) it largely improves analytical performance (e.g., sensitivity and simplicity) since the method establishes a direct relationship between the CRISPR-Cas12a system and the analyte; (3) it has different options in terms of signal readout, making it highly flexible to diverse detection platforms according to practical demand; and (4) it can be directly used in a clinic or a biology laboratory because of its high compatibility with the current ELISA platform.

EXPERIMENTAL SECTION

Detailed information of materials and instruments is given in the Supporting Information.

Synthesis of Apt-acDNA2/GNPs. The GNPs were synthesized according to a seed growth method.[20] Briefly, 30 mL of sodium citrate (2.2 mM) was heated to boiling under magnetic stirring. Then, 0.2 mL of $HAuCl_4$ (25 mM) was injected rapidly. When the solution turned soft pink, the solution temperature was reduced to 90 °C. Afterward, 0.2 mL of sodium citrate (60 mM) and 0.2 mL of $HAuCl_4$ solution (25 mM) were sequentially added (time delay ∼2 min) and incubated for 30 min. By repeating this process five times, large-sized gold nanoparticles (50 nm) could be obtained.

Apt-acDNA2/GNPs were prepared through a poly(ethylene glycol) (PEG)-assistant modification method.[21] Initially, the thiolated DNA strands were activated by 10 mM TCEP for 1 h at room temperature. Then, 5 μL of activated DNA strands (100 μM) was incubated with 490 μL of as-synthesized GNPs containing 2% PEG_{20000}. After vigorous agitation, 100 μL of NaCl (3 M) and 5 μL of complementary DNA (100 μM) were added to the mixture and the mixture was kept overnight at room temperature. Finally, the mixture was centrifuged and washed three times with *N*-(2-hydroxyethyl)piperazine-*N*′-ethanesulfonic acid (HEPES) buffer (10 mM, pH 7.4) containing 100 mM NaCl.

https://dx.doi.org/10.1021/acs.analchem.0c04687
Anal. Chem. XXXX, XXX, XXX−XXX

Preparation of Capture Aptamer/Capture Antibody-Modified Surface. The amino-modified capture aptamer was dissolved in immobilization buffer (10 mM HEPES, 1 mM ethylenediaminetetraacetic acid (EDTA), pH 8.5). The capture aptamer (100 μL; 0.4 μM) solution was added to a DNABIND strip well plate. The wells were coated with reactive NHS, which can covalently link with aptamer strands. After 2 h incubation at room temperature, the plate was washed with buffer to remove any unbound aptamers. Afterward, the wells were passivated by 3% bovine serum albumin (BSA) (150 μL) for 1 h at 37 °C and washed three times and stored at 4 °C for subsequent use. For antibody-modified plates, 100 μL of capture antibody (5 μg/mL) was added in a common 96-well plate and incubated overnight at 4 °C. After discarding the solution, the plate was washed using PBST buffer (0.05% Tween-20) and blocked using 3% BSA (150 μL) for 1 h at 37 °C. Finally, the plate was washed three times and stored at 4 °C for subsequent use.

Fluorescent Detection of Platelet-Derived Growth Factor-BB (PDGF-BB) Using ALCIA or Nano-ALCIA. Samples (100 μL) with varying concentrations of PDGF-BB were added to each capture aptamer-modified well. After 40 min incubation, the plate was washed three times. Then, 100 μL of the crRNA/Apt-acDNA1/Cas12a complex (5 nM) or Apt-acDNA2/GNPs (1 nM) was added to each well and incubated for 40 min at 37 °C. After washing the plates three times, 100 μL of ssDNA reporters (20 nM) was added to the enzyme complex adsorbed surface. After 25 min of incubation, the fluorescent signal is directly measured by a microreader. As for Nano-ALCIA, crRNA/Cas12a and ssDNA reporters were added to each well in succession. After 30 min of incubation, the fluorescent signal can be recorded and analyzed. Cleavage of ssDNA reporters was performed in the reaction buffer at 37 °C.

Colorimetric Detection of Adenosine Triphosphate (ATP) and Multiple Biomarkers Using Opti-ALCIA. For ATP detection, a split aptamer1 was first modified on the plate according to the above-mentioned protocol. Afterward, the wells were washed and incubated with ATP of varying concentrations and Apt-acDNA3/GNPs (2.5 nM) for 30 min at 37 °C, followed by another washing and addition of the crRNA/Cas12a complex (10 nM). Then, 100 μL of blocker DNA (20 nM) was added and incubated for another 30 min at 37 °C. The cleavage reaction was stopped by heating at 70 °C for 10 min. Then, 50 μL of DNAzyme (40 nM) was added and the plate was immediately chilled on ice for 10 min. Finally, 50 μL of TMB substrate was added and kept to react at room temperature to give rise to the colorimetric signal. The signal was recorded using a microreader. The detection of other biomarkers used the antibody-modified plates. The detection procedures were similar to ATP detection.

Stool samples (0.5 g) were dissolved in phosphate-buffered saline (PBS) (0.6 mL) buffer and then were vortexed for 30 s. After standing for 10 min at 4 °C, the samples were centrifuged (2000 rpm) for 5 min. Then, the supernatants (500 μL) were transferred into RNase-free tubes and were stored at 4 °C for subsequent use.

Electrochemical Detection of Tumor Cells Using E-ALCIA. For cell detection, 100 μL of Apt-acDNA4 (100 nM) strands were added to the wells with different cell numbers for 30 min at 37 °C. After removing unbound aptamers, the crRNA/Cas12a complex (5 nM) was introduced and incubated for another 15 min to form a ternary complex. Then, 100 μL of signal probe (1 μM) was added and cleaved for 25 min. In parallel, the clean gold electrode was subjected to 0.4 V for 5 min to ensure a reduced gold surface. When DNA cleavage was completed, the electrode was immersed in the well and incubated for 5 min under a potential of 0.4 V to accelerate DNA modification. Finally, the electrode was rinsed with phosphate buffer (PBS, pH 7.4) containing 0.1% sodium dodecyl sulfate (SDS) and then subjected to electrochemical measurements.

The electrochemical measurement was carried out in a typical three-electrode system by square wave voltammetry (SWV). The electrochemical signal of methylene blue (MB) was obtained in 10 mM Tris−HCl buffer (pH 7.4) at −0.27 V.

RESULTS AND DISCUSSION

As a proof-of-concept study, we first used platelet-derived growth factor-BB (PDGF-BB), a growth factor protein found in human platelets, as the model analyte. PDGF-BB has two identical subunits that can bind with a pair of well-characterized aptamers ($Apt_{PDGF-BB}$). So, one aptamer, as a capture strand, is modified on the plate substrate, and the other is employed as a detection strand that was extended from the 3′ end of acDNA (Apt-acDNA1, Figure 1A). Although PDGF-BB has been extensively used as a model target for biosensing, its detection using the CRISPR/Cas system has not been achieved. The sensing principle of the proposed ALCIA for PDGF-BB detection is presented in Figure 1A. The detection method is straightforward, which involved the formation of a classic sandwich-type structure and Cas12a-catalyzed cleavage of ssDNA reporters, producing amplified fluorescence signals. Thus, the protocol of ALCIA is a mirror to traditional ELISA, which can be directly imposed on the current ELISA platform. Of note, the solid substrate used here is a commercially available DNA binding plate, which allows covalent immobilization to amine-modified oligonucleotides via binding to *N*-oxysuccinimide (NOS) groups.

We investigated the collateral cleavage activity of the crRNA/Apt-acDNA1/Cas12a complex using a common acDNA strand without the $Apt_{PDGF-BB}$ sequence as a positive control. As shown in Figure 1B, the collateral cleavage activity of Cas12a was only activated when Cas12a/crRNA/acDNA/magnesium ions were present simultaneously. Moreover, there was no obvious difference between samples using either acDNA or acDNA1, indicating that the addition of the aptamer sequence on acDNA did not affect the trans-cleavage activity of Cas12a. After its activation by acDNA, crRNA/acDNA/Cas12a cleaved ssDNA reporters with very high catalytic efficiency and could produce detectable fluorescent signals after 30 min incubation with a detection limit of 0.75 pM (Figure 1C). This sensitivity was about 80-fold higher than that of horseradish peroxidase (HRP), a widely used enzyme for colorimetric signal readout, which produced detectable colorimetric signals above 60 pM (Figure S1).

Next, we investigated the recognition ability of the crRNA/Apt-acDNA1/Cas12a complex using $Apt_{PDGF-BB}$ as the positive control and crRNA/acDNA1/Cas12a complex as the negative control. To demonstrate this, acDNA1, Apt-acDNA1, and Cas12a were labeled with red quantum dots (rQDs, $\lambda_{emission}$ = 560 nm), respectively, using NHS chemistry (Figure S2). Thus, their binding on the PDGF-BB-modified solid surface could be directly observed through a confocal microscope. As depicted in Figure 1D, without the $Apt_{PDGF-BB}$ sequence, the crRNA/acDNA1/Cas12a complex could not bind to the

https://dx.doi.org/10.1021/acs.analchem.0c04687
Anal. Chem. XXXX, XXX, XXX−XXX

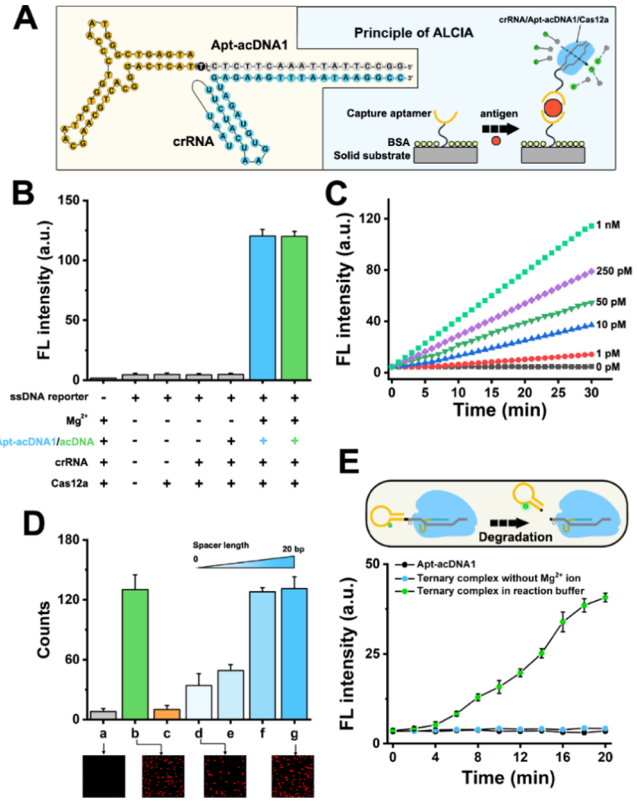


Figure 1. (A) Sensing principle of ALCIA for PDGF-BB detection (right) and the structure of Apt-acDNA1 (left). The sequence of the used Apt-acDNA1 contains four regions: yellow sequence (PDGF-BB aptamer), black sequence (spacer), gray sequence (acDNA), and blue sequence (crRNA). (B) Evaluation of collateral cleavage activity of CRIPSR/Cas12a in the presence of different components. [Cas12a] = 1 nM; [crRNA] = 1 nM; [Apt-acDNA1] = 1 nM; [ssDNA reporter] = 20 nM. The reaction was performed in the reaction buffer for 30 min at 37 °C. The fluorescence intensity at 520 nm was recorded with an extinction light at 494 nm. (C) Evaluation of the sensitivity of CRIPSR/Cas12a with a function of reaction time. (D) Effects of spacer length of Apt-acDNA1 (columns d−g: 0, 5, 10, and 20 bp) on recognition efficiency of the ternary complex. Column a, blank plate; column b, PDGF-BB + Apt-acDNA1/rQD; and column c, PDGF-BB + acDNA1/rQD. (E) Investigation of the stability of the crRNA/Apt-acDNA1/Cas12a complex under different buffer conditions. Error bars show the standard deviations of three independent measurements.

surface (column c), indicating that its nonspecific adsorption was very weak. In sharp contrast, when crRNA/Apt-acDNA1/Cas12a was used, many red dots appeared on the surface (column d), suggesting the adsorption of the complex. However, it was worth noting that that the overall signal was about 3.8-fold less than the positive control group using pure $Apt_{PDGF-BB}$ (column b). This reduced recognition capacity was probably due to the steric hindrance induced by the large size of Cas12a, which disturbed the interaction between the aptamer and PDGF-BB. To address this problem, we introduced a spacer sequence of $(dT)_n$ between the aptamer region and acDNA region in Apt-acDNA1. As expected, we observed that the binding capacity of the ternary complex was obviously improved after the introduction of a spacer (columns d−g), which reached a plateau using a 10 bp spacer.

Before its final use, the stability of the crRNA/Apt-acDNA1/Cas12a complex was also tested because the Apt-acDNA1 strand also contains a ssDNA sequence (i.e., loop and spacer structure that may be attacked by Cas12a). To test this, we labeled a pair of a fluorophore and a quencher (FAM and BHQ-1) at Apt-acDNA1 (Figure 1E), and the fluorescence of 5(6)-carboxyfluorescein (FAM) was initially quenched. After the formation of the ternary complex, we observed that the fluorescence signal rapidly increased when the complex was in the reaction buffer (Figure 1E), indicating the cleavage of Apt-acDNA1, which is adverse to bioanalysis. There are two possible methods to solve this problem: (1) we can use Apt-acDNA1 and crRNA/Cas12a independently; however, it may bring an additional incubation step; (2) considering the collateral cleavage activity of Cas12a heavily relies on the concentration of magnesium ions (Figures 2B and S3), we can

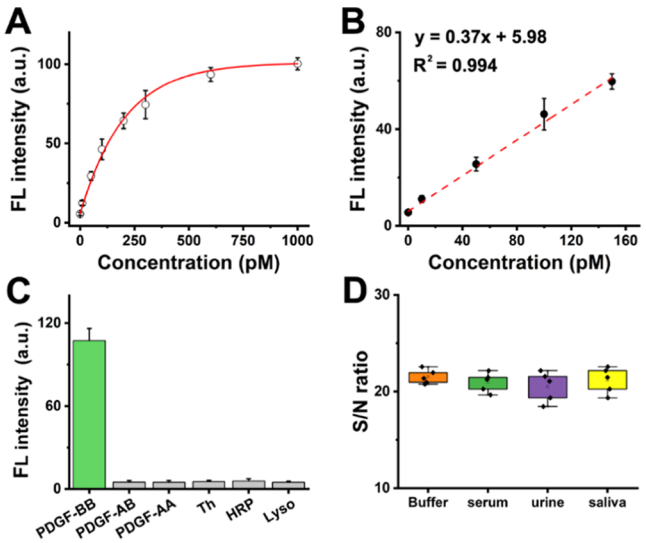


Figure 2. Use of ALCIA for detection of PDGF-BB. (A) Fluorescence responses of different PDGF-BB concentrations ranging from 0 to 1000 pM. (B) Linear trend line of fluorescence intensity induced by PDGF-BB concentrations between 0 and 150 pM. (C) Specificity of ALCIA for detection of PDGF-BB. (D) Signal-to-noise (S/N) ratio of the ALCIA detecting PDGF-BB spiked in different biofluids.

simply modulate the buffer component without the addition of magnesium ion(II), thus keeping the stability of the complex before activation of enzyme activity (Figure S4).

Next, the analytical performance of ALCIA was studied. The fluorescent intensity was dependent on the concentration of PDGF-BB. The detection range of PDGF-BB was 0−150 pM with a detection limit of 1.57 pM according to 3σ/slope (Figure 2B), which was about 40-fold lower than the traditional ELISA kit (Figure S5) and comparable to previously reported amplified PDGF-BB fluorescent sensors.[22,23] Of note, the detection range was relatively narrow, which was probably due to the high catalytic capacity of Cas12a and the low concentration of reporter DNA. As a result, the responsive signal reached the plateau rapidly. Furthermore, control proteins, such as PDGF-AB, PDGF-AA, thrombin (Th), HRP, and lysozyme (Lyso), only led to very weak responses, suggesting the high selectivity of the proposed ALCIA (Figure 2C). Furthermore, the proposed assay could also work well in biological media by spiking PDGF-BB in serum, urine, and saliva (Figure 2D), which further revealed the performance of ALCIA in real samples.

Considering the abundance of many biomarkers is extremely low at the early stages of the disease; therefore, we wonder if

https://dx.doi.org/10.1021/acs.analchem.0c04687
Anal. Chem. XXXX, XXX, XXX−XXX

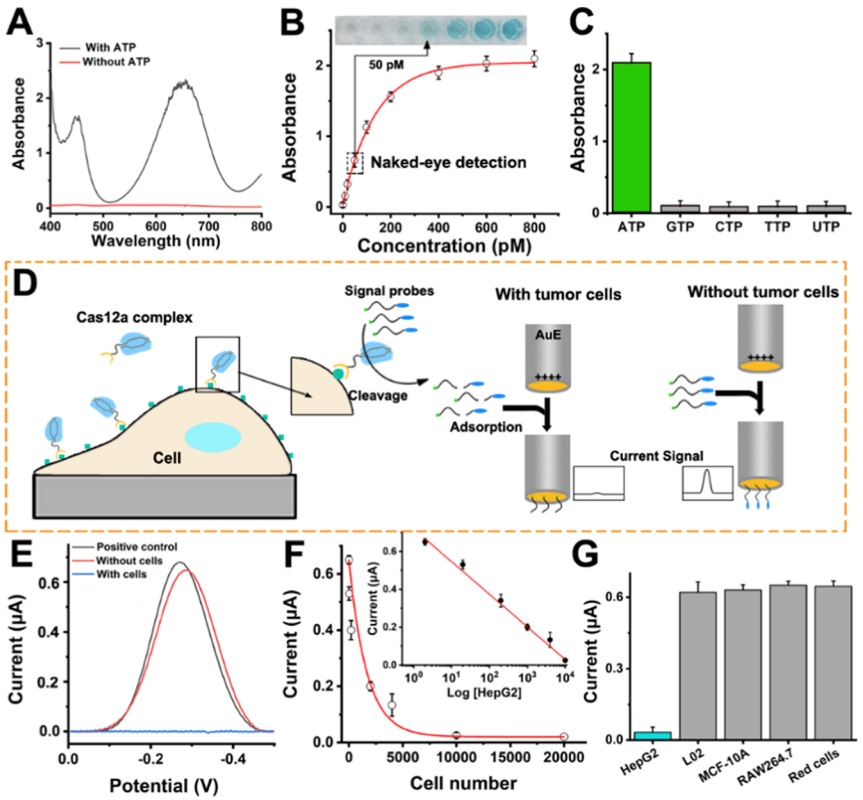


Figure 3. Use of Opti-ALCIA and E-ALCIA for detection of ATP and HepG2 cells, respectively. (A) Feasibility study of the Opti-ALCIA for ATP detection. [ATP] = 1 nM. (B) Colorimetric responses of different ATP concentrations ranging from 0 to 800 pM. The inset indicates the colorimetric responses for ATP detection (from left to right: 0, 5, 20, 50, 100, 200, and 400 pM). (C) Selectivity of the Opti-ALCIA-based ATP assay based on the colorimetric reaction. NC (negative control): detection reaction without ATP. [NTP] = 1 nM. (D) Schematic illustration of E-ALCIA for HepG2 cell detection. (E) Feasibility study of the proposed E-ALCIA under different conditions. (F) Current responses of different cell numbers ranging from 0 to 2×10^4 cells. The inset indicates the linear trend of the electrochemical assay for the detection of HepG2 cells ranging from 20 to 10 000 cells. (G) Selectivity of the E-ALCIA-based tumor cell assay. All cell numbers are fixed to be 1×10^4.

appropriate signal amplification methods can be integrated into ALCIA for improving sensing performance. Hence, we design a spherical nucleic acid-based nanoprobe for signal amplification, avoiding the use of an expensive and unstable enzyme reported by previous reports.[10] As shown in Figure S6A, Apt-acDNA2 is mainly composed of two DNA strands: an anchor strand and a recognition strand. The anchor strand contains a thiol group, an oligo(ethylene glycol) (OEG) linker, and a short DNA strand containing a PAM sequence. The recognition strand contains three regions: an aptamer strand to recognize PDGF-BB specifically, a poly(T) spacer, and a complementary strand to the anchor strand. Specifically, the OEG linker plays a critical role in improving nanoparticle stability and facilities DNA modification with high loading capacity, and the DNA duplex is employed as acDNA to activate Cas12a, which can be cleaved at the designed sites.

Typically, one gold nanoparticle (GNP, d = 50 nm) carries thousands of Apt-acDNA2 molecules, so remarkable signal amplification may be envisioned. The nanoprobe (referred as Apt-acDNA2/GNPs) is composed of a GNP core and an Apt-acDNA2 shell. The protocol of this nanoprobe-based ALCIA (Nano-ALCIA) is also akin to traditional ELISA (Figure S6B). After formation of a sandwich-type structure, crRNA/Cas12a and reporter DNA are added to the well. Thus, crRNA/Cas12a complexes bind to Apt-acDNA2 exhibited on the GNPs, and consequently, the cis-cleavage activity of Cas12a is activated immediately, leading to the cleavage of Apt-acDNA2 strands and the release of crRNA/acDNA/Cas12a into the solution. Finally, the activated Cas12a enzymes can execute their trans-cleavage capacity to degrade reporter DNA in the solution, thereby producing amplified fluorescent signals because one antigen can activate thousands of Cas12a enzymes.

To test this strategy, we first prepared the nanoprobe through a previously reported method. The successful preparation of Apt-acDNA2/GNPs was characterized by transmission electron microscopy (TEM), UV−vis absorption spectroscopy, and dynamic light scattering (DLS) (Figure S7). The number of DNA strands on each GNP was estimated to be 1092 according to the established fluorescent method.

The binding capacity of Apt-acDNA2/GNPs toward the PDGF-BB-modified surface was evaluated by scanning electron microscopy (SEM). As shown in Figure S8, bare GNPs and GNP modified with random DNA strands could not bind to the surface. As a comparison, a large number of Apt-acDNA2/GNPs adsorbed on the PDGF-BB-modified surface rather than the PDGF-AB-modified surface, indicating that the recognition capacity of Apt-acDNA2/GNPs was well retained. The reason to decouple Apt-acDNA2/GNPs and crRNA/Cas12a in this strategy was mainly due to the large size of the formed nanocomplex, which hampered its diffusion toward the sensing surface (data not shown).

Next, we determined time-dependent fluorescence responses of ssDNA reporters in the presence of crRNA/Cas12a, Apt-acDNA2/GNPs, crRNA/Apt-acDNA2/Cas12a, and both of Apt-acDNA2/GNPs and crRNA/Cas12a. As shown in Figure S6C, no fluorescence increased over time, so crRNA/Cas12a

https://dx.doi.org/10.1021/acs.analchem.0c04687
Anal. Chem. XXXX, XXX, XXX−XXX

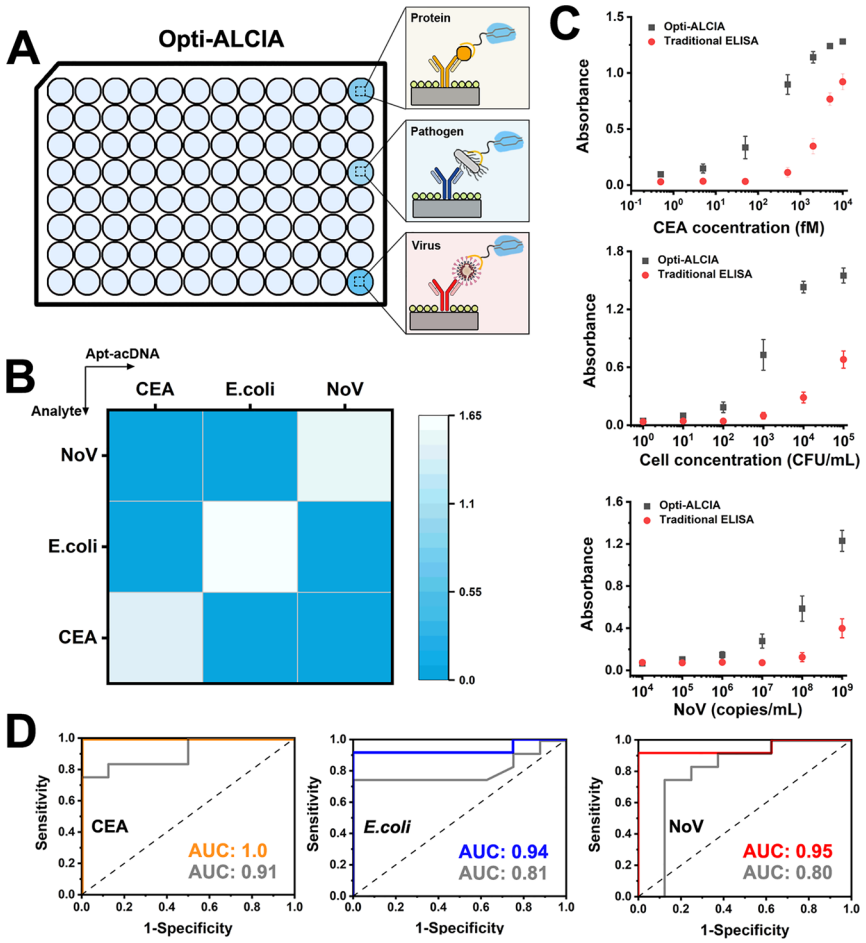


Figure 4. Use of Opti-ALCIA for detection of biomarkers in real samples. (A) Schematic illustration of a combination of capture antibody-modified plates and the crRNA/Apt-acDNA/Cas12a complex for detection of biomarkers. (B) Heat map of the specific detection of three biomarkers. All combinations were tested. The values are the average colorimetric signal of three replicates at 30 min. (C) Linear curves of the three kits for analyte detection. The color value was recorded at 450 nm after 20 incubation. (D) Receiver operating characteristic (ROC) curve analysis of validation cohort. Colorful curves result from the results of Opti-ALCIA, and gray curves result from the results of traditional ELISA.

and Apt-acDNA2 could not cleave the reporters. Nevertheless, the addition of Apt-acDNA2 (1 pM) to the crRNA/Cas12a complex led to slight fluorescence enhancement, suggesting that ssDNA reporters were slowly cleaved due to the inefficient supply of acDNA. To our surprise, upon simultaneous introduction of both Apt-acDNA2/GNPs (1 pM) and crRNA/Cas12a gave rise to a more dramatic increase of fluorescence and rapidly reached the plateau within 30 min. This observation reveals that the nanoprobe is more effective on activation of Cas12a compared with a linear acDNA strand due to the increased number of acDNA strands on nanoparticles. Also, of note, in this strategy, we took advantage of a DNA duplex as acDNA, and thus, the *cis*-activity of Cas12a would be first activated, resulting in the release of Cas12a from the nanoparticle surface, which could leave plenty of room on GNPs for other enzyme molecules' binding. If the DNA duplex region was replaced by single-stranded acDNA, the amplification effect obviously reduced (Figure S9).

By utilizing this nanoprobe, the involved GNP-ALCIA showed an enhanced performance for PDGF-BB detection. Figure 3D shows that the fluorescence signal increased with increasing PDGF-BB concentrations from 1 to 400 fM with a limit of detection (LOD) of 550 aM, which is approximate 10^3 times lower than that of the above-mentioned common ALCIA. Moreover, the sensitivity of Nano-ALCIA is enhanced more than 100-fold compared to other fluorescent PDGF-BB biosensors (Table S2), which is one of the most sensitive methods for PDGF-BB detection.

Despite the above success, fluorescent signal readout usually requires sophisticated instruments and expensive fluorophore labels, while some detection platforms such as colorimetric or electrochemical signal output have been well recognized due to their simplicity and low cost, which are highly desirable for resource-limited settings. Therefore, we turned our attention to achieving optical detection through the naked eye (denoted Opti-ALCIA) and electrochemical detection (denoted E-ALCIA). To do so, an HRP-mimicking DNAzyme with high enzymatic efficiency is employed as a signal generator and a blocker strand was designed to inactivate the DNAzyme (Figure S10). In the absence of the analyte, the blocker strand will hybrid with DNAzyme, thus completely inhibiting its activity. However, the presence of the analyte will bring Cas12a onto the solid surface, thus resulting in the cleavage of blocker strands. Then, the well was heated to inactivate Cas12a, and subsequently, the DNAzyme solution was added for the hybridization reaction. Finally, hemin was added into the well, and unblocked DNAzyme oxidized the colorless tetramethylbenzidine (TMB) into colored products in the presence of H_2O_2. As a result, final results could be judged by direct observation of color change in the reaction solution.

https://dx.doi.org/10.1021/acs.analchem.0c04687
Anal. Chem. XXXX, XXX, XXX−XXX

To test the feasibility of this strategy, we designed an ATP sensing strategy, which is based on Apt-acDNA3-modified GNPs (Apt-acDNA3/GNPs) containing a split aptamer (Figure S11). Using GNPs can significantly improve the binding affinity of the split aptamer, thus improving analytical performance. Figure 3A shows that 20 nM DNAzyme could efficiently catalyze the oxidation of the TMB substrate and produce remarkable colorimetric signals. Nevertheless, in the absence of block strands (20 nM), the activity of DNAzyme was completely diminished, so the solution remained transparent. When the block strand was pretreated with Apt-acDNA3/GNPs and the crRNA/Cas12a complex for 30 min, the activity of DNAzyme was entirely restored and the saturated signal was achieved, demonstrating the feasibility of the proposed Opti-ALCIA.

Figure 3B shows that the proposed Opti-ALCIA can also detect the ATP concentration. The LOD for the ATP detection was found to be 0.14 pM, which was 1.5×10^6-fold lower than that of a previously reported Cas12a-based fluorescent sensor (0.21 μM).[12] Impressively, the method allows naked-eye detection of ATP as low as 50 pM, which is more sensitive than other colorimetric assays. In addition, Opti-ALCIA showed good selectivity for analogous analytes since control samples containing CTP, GTP, and TTP did not produce any responsive signals (Figure 3C).

An electrochemical sensor (E-sensor) is another widely used cost-effective detection platform. To construct an E-ALCIA, Apt-acDNA4 containing an AS1411 aptamer, specifically binding with nucleolin highly expressed on the tumor cell membrane, was designed. As shown in Figure 3D, in the presence of HepG2 cells, crRNA/Apt-acDNA4/Cas12a can freely bind to the surface of tumor cells through the aptamer−nucleolin interaction. Then, an electrochemical signal strand, consisting of a thiol group, a poly(T) spacer, and a methylene blue (MB) group, is introduced into the system and can be rapidly cleaved by Cas12a. Thus, the MB groups cannot be firmly attracted onto the gold electrode surface and are easily washed away, thereby resulting in reduced current signals. In contrast, in the absence of HepG2 cells, no ternary complex is adsorbed on the cell surface, so the signal strands can be retained in the solution. Thus, intact signal strands can be rapidly modified on the electrode surface under positive potential, giving rise to the current signal.

Figure 3E shows that a large current signal at −0.27 V could be observed after incubating electrodes with signal strands applying a positive voltage (+0.4 V) for 30 s, indicating the rapid immobilization of DNA strands on the electrode. Of note, although thiolated DNA can firmly adsorb onto the gold surface via Au−S chemistry, this process usually takes a relatively long time (several hours). By applying a positive potential, negatively charged DNA can be rapidly attracted onto gold surface, enabling rapid immobilization within several minutes. We also found that the current signal dramatically dropped (∼14 nA) in the presence of target cells and enzyme complex, indicating the efficient cleavage of signal strands. However, a large current signal was observed without target cells, which was due to the assembly of signal strands on the electrode, indicating the feasibility of the electrochemical strategy. Also, the binding of the crRNA/Apt-acDNA4/Cas12a complex to HepG2 cells was confirmed by confocal microscopy (Figure S12). The current signal decreased according to the increasing number of HepG2 cancer cells from 20 cells to 10 000 cells (Figure 3F). The LOD for the HepG2 cell detection was found to be 20 cells, which was better than other fluorescent methods for the same cell. Again, this method exhibited impressive selectivity for other cells. The result of the sample that contained HepG2 cells was distinctively different from the unintended targets: MCF-10A (normal breast epithelial cells), L02 (normal hepatocyte), RAW264.7 cells (macrophage cells), and red cells (Figure 3G).

Considering many biomarkers only have one selected aptamer, we attempted to introduce other recognition molecules (i.e., antibody) to the detection system for further broadening its real applications. As shown in Figure 4A, different disease biomarkers may be detected using a capture antibody-modified polystyrene (PS) plate and aptamer-linked Cas12a cooperatively. Similar to the traditional immunoassay, the antibody can be immobilized onto the PS surface via hydrophobic interaction and the impurities in the assay can be easily removed by buffer washing. To demonstrate this, we constructed three Opti-ALCIA kits for the detection of three analytes, including protein [carcino-embryonic antigen (CEA)], bacterium [*Escherichia coli* O157:H7], and virus (norovirus, NoV). Specifically, CEA is a well-recognized tumor biomarker for the diagnosis of colon cancer. *E. coli* O157:H7 is a foodborne pathogen that causes food poisoning. As for norovirus (NoV), it is commonly referred to as "stomach flu", which usually causes diarrhea and emesis.

The orthogonality of all three kits was first tested using corresponding capture antibodies and Apt-acDNA strands. The resulting optical signals demonstrated strong orthogonality and little cross talk (Figure 4B), indicating the excellent selectivity of the proposed method. The sensitivity was next evaluated. By utilizing corresponding Apt-acDNA/GNPs, excellent sensitivity was achieved (Figure 4C), whose LOD exhibited 100- to 1000-fold improvement compared to traditional ELISA methods. We also applied the Opti-ALCIA to detect these biomarkers in complex biofluids. Twenty samples, including serum, milk, and stool, were spiked with CEA, *E. coli*, and NoV particles, respectively. Consequently, as shown in Figure 4D, our method achieved sufficiently high accuracy with area under curve (AUC) values of receiver operating characteristic (ROC) curves of 1.0, 0.94, and 0.95 for CEA-, *E. coli*-, and NoV-spiked samples, respectively. As a comparison, traditional ELISA, employed as a control technique, only showed a moderate accuracy with AUC values of 0.91, 0.81, and 0.8, respectively. The detailed detection information is shown in Table S3−S6.

We chose the appropriate clinical threshold value that maximizes the sensitivity and the specificity at the same time (black dotted line, Figure S13). Impressively, 19 of 20 NoV cases were successfully differentiated by the Opti-ALCIA; that is, the A_{450} exceeded the detection threshold (A_{450} = 0.011). Meanwhile, NoV-negative samples were below the cutoff value, revealing the excellent sensitivity (95%) and specificity (100%) of the proposed assay.

CONCLUSIONS

In summary, we have described a simple strategy to make use of the CRISPR/Cas12a system for biosensing. Through the rational design of acDNA, different kinds of analytes such as proteins, small molecules, and tumor cells can be detected by the proposed ALCIA. The proposed methods appear to have several interesting features for analytical applications: (1) they are highly versatile, which can be used to detect a variety of analytes by simply replacing them with corresponding

https://dx.doi.org/10.1021/acs.analchem.0c04687
Anal. Chem. XXXX, XXX, XXX−XXX

aptamers; (2) they are highly sensitive, which are able to detect sub-attomolar proteins using easy-to-fabricate nanoprobes; (3) they can be adapted into currently available detection platforms, e.g., microplate reader, greatly facilitating their real applications; and (4) they are highly flexible, which can be integrated with different detection platforms. Those characteristics are different from previously reported CRISPR/Cas12a-based sensing methods that mainly rely on fluorescence readout with reduced transduction efficiency because we have established a direct correlation between the catalysis systems with recognition elements (i.e., aptamers), thus greatly improving the working efficiency of the detection platform (Table S7). Furthermore, inspired by this strategy, other functional elements or portable devices (e.g., paper-based devices or microfluidic devices) may be introduced into this method for point-of-care (POC) medical applications.

■ ASSOCIATED CONTENT

Supporting Information

The Supporting Information is available free of charge at https://pubs.acs.org/doi/10.1021/acs.analchem.0c04687.

Information of materials and instruments, sequence of the used nucleic acids, detailed detection procedures, HRP activity, modification of rQDs, effects of Mg^{2+} ions on enzyme activity, commercial ELISA kit for PDGF-BB detection, characterization of the nanoprobe, adsorption of GNPs on a plate, amplification effect of using Apt-acDNA2, scheme of Opti-ALCIA and split ATP aptamer, and adsorption of the Cas12a complex on the cell membrane (PDF)

■ AUTHOR INFORMATION

Corresponding Authors

Feng Wang − *School of Food and Biological Engineering, Hefei University of Technology, Hefei 230009, P. R. China*; Email: fengw420@hfut.edu.cn

Chao Li − *School of Food and Biological Engineering, Hefei University of Technology, Hefei 230009, P. R. China*; orcid.org/0000-0002-2552-413X; Email: lchao@hfut.edu.cn

Authors

Hui Li − *School of Food and Biological Engineering, Hefei University of Technology, Hefei 230009, P. R. China*; orcid.org/0000-0003-3346-6133

Menglu Li − *State Key Laboratory of Pharmaceutical Biotechnology, School of Life Sciences, Nanjing University, Nanjing 210023, P. R. China*

Yucai Yang − *Department of Oncology, The Second Affiliated Hospital of Anhui Medical University, Hefei 230601, P. R. China*; orcid.org/0000-0001-6634-3215

Fei Wang − *School of Food and Biological Engineering, Hefei University of Technology, Hefei 230009, P. R. China*

Complete contact information is available at: https://pubs.acs.org/10.1021/acs.analchem.0c04687

Author Contributions

‖H.L. and M.L. contributed equally.

Notes

The authors declare no competing financial interest.

■ ACKNOWLEDGMENTS

This work was supported by the National Natural Science Foundation of China (Grant Nos. 21804069, 81802978, and 31971314), the Distinguished Youth Foundation of Anhui Province (1808085J05), and the Fundamental Research Funds for the Central Universities of China (Grant No. JZ2017HGPA0164).

■ REFERENCES

(1) Mali, P.; Yang, L.; Esvelt, K. M.; Aach, J.; Guell, M.; DiCarlo, J. E.; Norville, J. E.; Church, G. M. *Science* **2013**, *339*, 823−826.

(2) Hsu, P. D.; Lander, E. S.; Zhang, F. *Cell* **2014**, *157*, 1262−1278.

(3) Gootenberg, J. S.; Abudayyeh, O. O.; Lee, J. W.; Essletzbichler, P.; Dy, A. J.; Joung, J.; Verdine, V.; Donghia, N.; Daringer, N. M.; Freije, C. A.; Myhrvold, C.; Bhattacharyya, R. P.; Livny, J.; Regev, A.; Koonin, E. V.; Hung, D. T.; Sabeti, P. C.; Collins, J. J.; Zhang, F. *Science* **2017**, *356*, 438−442.

(4) Kellner, M. J.; Koob, J. G.; Gootenberg, J. S.; Abudayyeh, O. O.; Zhang, F. *Nat. Protoc.* **2019**, *14*, 2986−3012.

(5) Chen, J. S.; Ma, E.; Harrington, L. B.; Da Costa, M.; Tian, X.; Palefsky, J. M.; Doudna, J. A. *Science* **2018**, *360*, 436−439.

(6) Li, S.-Y.; Cheng, Q.-X.; Liu, J.-K.; Nie, X.-Q.; Zhao, G.-P.; Wang, J. *Cell Res.* **2018**, *28*, 491−493.

(7) Swarts, D. C.; Jinek, M. *Mol. Cell* **2019**, *73*, 589−600.

(8) Teng, F.; Guo, L.; Cui, T.; Wang, X.-G.; Xu, K.; Gao, Q.; Zhou, Q.; Li, W. *Genome Biol.* **2019**, *20*, No. 132.

(9) Wang, B.; Wang, R.; Wang, D.; Wu, J.; Li, J.; Wang, J.; Liu, H.; Wang, Y. *Anal. Chem.* **2019**, *91*, 12156−12161.

(10) Yuan, C.; Tian, T.; Sun, J.; Hu, M.; Wang, X.; Xiong, E.; Cheng, M.; Bao, Y.; Lin, W.; Jiang, J.; Yang, C.; Chen, Q.; Zhang, H.; Wang, H.; Wang, X.; Deng, X.; Liao, X.; Liu, Y.; Wang, Z.; Zhang, G.; Zhou, X. *Anal. Chem.* **2020**, *92*, 4029−4037.

(11) Liang, M.; Li, Z.; Wang, W.; Liu, J.; Liu, L.; Zhu, G.; Karthik, L.; Wang, M.; Wang, K.-F.; Wang, Z.; Yu, J.; Shuai, Y.; Yu, J.; Zhang, L.; Yang, Z.; Li, C.; Zhang, Q.; Shi, T.; Zhou, L.; Xie, F.; Dai, H.; Liu, X.; Zhang, J.; Liu, G.; Zhuo, Y.; Zhang, B.; Liu, C.; Li, S.; Xia, X.; Tong, Y.; Liu, Y.; Alterovitz, G.; Tan, G.-Y.; Zhang, L.-X. *Nat. Commun.* **2019**, *10*, No. 3672.

(12) Xiong, Y.; Zhang, J.; Yang, Z.; Mou, Q.; Ma, Y.; Xiong, Y.; Lu, Y. *J. Am. Chem. Soc.* **2020**, *142*, 207−213.

(13) Zhao, X.; Zhang, W.; Qiu, X.; Mei, Q.; Luo, Y.; Fu, W. *Anal. Bioanal. Chem.* **2020**, *412*, 601−609.

(14) Chen, Q.; Tian, T.; Xiong, E.; Wang, P.; Zhou, X. *Anal. Chem.* **2020**, *92*, 573−577.

(15) Bruch, R.; Urban, G. A.; Dincer, C. *Trends Biotechnol.* **2019**, *37*, 791−792.

(16) Engvall, E.; Perlmann, P. *Immunochemistry* **1971**, *8*, 871−874.

(17) Srinivas, P. R.; Kramer, B. S.; Srivastava, S. *Lancet Oncol.* **2001**, *2*, 698−704.

(18) Acharya, A. P.; Nafisi, P. M.; Gardner, A.; MacKay, J. L.; Kundu, K.; Kumar, S.; Murthy, N. *Chem. Commun.* **2013**, *49*, 10379−10381.

(19) Keefe, A. D.; Pai, S.; Ellington, A. *Nat. Rev. Drug Discovery* **2010**, *9*, 537−550.

(20) Bastus, N. G.; Comenge, J.; Puntes, V. *Langmuir* **2011**, *27*, 11098−11105.

(21) Zhang, X.; Servos, M. R.; Liu, J. *J. Am. Chem. Soc.* **2012**, *134*, 9910−9913.

(22) Li, H.; Wang, M.; Wang, C.; Li, W.; Qiang, W.; Xu, D. *Anal. Chem.* **2013**, *85*, 4492−4499.

(23) Yang, C. J.; Jockusch, S.; Vicens, M.; Turro, N. J.; Tan, W. H. *Proc. Natl. Acad. Sci. U.S.A.* **2005**, *102*, 17278−17283.

https://dx.doi.org/10.1021/acs.analchem.0c04687
Anal. Chem. XXXX, XXX, XXX−XXX